

Article

Reactive Transport Modeling of Chemical Stimulation Processes for an Enhanced Geothermal System (EGS)

Li Ma ¹, Zhenpeng Cui ², Bo Feng ², Xiaofei Qi ³, Yuandong Zhao ¹ and Chaoyu Zhang ^{4,*}

¹ Mudanjiang Natural Resources Comprehensive Survey Center of China Geological Survey, Mudanjiang 157021, China; mali@mail.cgs.gov.cn (L.M.); zhaoyuandong@mail.cgs.gov.cn (Y.Z.)

² Engineering Research Center of Geothermal Resources Development Technology and Equipment, Ministry of Education, Jilin University, Changchun 130026, China; zhenpeng971202@foxmail.com (Z.C.); fengbo234@126.com (B.F.)

³ No. 2 Exploration Team Hebei Bureau of Coal Geological Exploration, Xingtai 054001, China; xfqi2012@126.com

⁴ Chinese Academy of Natural Resources Economics, Beijing 100035, China

* Correspondence: cyzhang@canre.org.cn

Abstract: An enhanced geothermal system is a kind of artificial geothermal system, which can economically exploit geothermal energy from deep thermal rock mass with low permeability by artificially created geothermal reservoirs. Chemical stimulation refers to a reservoir permeability enhancement method that injects a chemical stimulant into the fractured geothermal reservoir to improve the formation permeability by dissolving minerals. In this study, a reactive solute transport model was established based on TOUGHREACT to find out the effect of chemical stimulation on the reconstruction of a granite-hosted enhanced geothermal system reservoir. The results show that chemical stimulation with mud acid as a stimulant can effectively improve the permeability of fractures near the injection well, the effective penetration distance can reach more than 20 m after 5 days. The improvement of porosity and permeability was mainly caused by the dissolution of feldspar and chlorite. The permeability enhancement increased with the injection flow rate and HF concentration in the stimulant, which was weakly affected by the change in injection temperature. The method of chemical enhancement processes can provide a reference for subsequent enhanced geothermal system engineering designs.

Keywords: enhanced geothermal system; chemical stimulation; reactive transport modeling; TOUGHREACT



Citation: Ma, L.; Cui, Z.; Feng, B.; Qi, X.; Zhao, Y.; Zhang, C. Reactive Transport Modeling of Chemical Stimulation Processes for an Enhanced Geothermal System (EGS). *Energies* **2023**, *16*, 6229. <https://doi.org/10.3390/en16176229>

Academic Editor: Massimo Dentice D'Accadia

Received: 6 August 2023

Revised: 21 August 2023

Accepted: 24 August 2023

Published: 27 August 2023



Copyright: © 2023 by the authors. Licensee MDPI, Basel, Switzerland. This article is an open access article distributed under the terms and conditions of the Creative Commons Attribution (CC BY) license (<https://creativecommons.org/licenses/by/4.0/>).

1. Introduction

Compared with other renewable energy and conventional energy, as an ideal new clean energy, geothermal energy has many advantages in engineering and environmental aspects, such as no seasonal dependence, small mining area, etc. [1,2]. The enhanced geothermal system (EGS) is a kind of artificial geothermal system to economically extract geothermal energy from low-permeability rock mass by using the method of artificially forming a geothermal reservoir [3]. The performance of EGS mainly depends on the development of reservoir fracture networks and the hydraulic connection between injection/production wells [4,5]. The commonly used methods for reservoir stimulation currently include hydraulic shearing, thermal stimulation [6], and chemical stimulation [7]. Chemical stimulation refers to the injection of chemical stimulants into the reservoir at a relatively low injection pressure, relying on the dissolution effect of the stimulants on minerals to improve the permeability of reservoir fractures [8]. Compared to traditional reservoir reconstruction methods, chemical stimulation has gradually gained attention due to its good penetration performance and low risk of inducing earthquakes [9,10].

Chemical stimulation has been widely used for oil and gas reservoir stimulation since 1895 and was first applied to improve the permeability of the EGS reservoir in Fenton

Hill, USA in 1976 [11]. The application result of the Fenton Hill project indicated that a single alkaline chemical stimulant cannot meet the requirements of actual sites for EGS reservoir reconstruction [12]. The Soultz EGS project in France used four kinds of chemical stimulants, including HCl, mud acid (HCl + HF), NTA, and organic clay acid, to enhance the permeability of geothermal wells and near-well reservoirs. The results showed that chemical stimulation can effectively reconstruct EGS reservoirs, but the dissolution effect of a single NTA was weak [13]. The fjällbacka EGS project in Sweden is the earliest practical site to use mud acid as a chemical stimulant. In 1988, the Fjb3 well was acidified to dissolve the blocked minerals in the reservoir fractures with significant results, indicating that soil acid can be used as an effective chemical stimulant for EGS reservoir reconstruction [14].

In recent years, scholars in related fields have conducted many indoor experiments and numerical simulations to analyze and predict the practical application effects of chemical stimulation and to explore the mechanism. Fei et al. [15] explored the effect of HF and organic acid on sandstone reservoir acidification through indoor experiments, as well as the effects of different factors. Na et al. [16] carried out a dynamic experiment under high temperature and high pressure and used a numerical simulator to fit and verify the experimental results. The results showed that the low-concentration mud acid with added particle stabilizer had a good reconstruction effect on the tuff reservoir. Luo et al. [17] conducted a long-term acid–rock reaction experiment and permeability test on samples after the reaction. The result showed that the permeability of granite cores modified with 12% HCl + 5% HF can be increased by four orders of magnitude. Yue et al. [18] established a reaction kinetics model with multiple minerals based on the results of a static corrosion experiment and calibrated relevant parameters, providing important reference for subsequent experimental designs and numerical simulations.

The chemical stimulation application experiment at the site scale is hard to carry out due to the technical difficulty and high cost of practical operation and monitoring. However, the results of indoor experiments are limited by scale effects and other issues, which may differ from the actual application effect of stimulation. Therefore, numerical simulation is considered an effective means to explore the reaction process between deep geothermal fluids and rock minerals. Xu et al. [19] simulated the chemical stimulation process of injection wells in a geothermal site, and the result showed that the high pH chelating solution can effectively dissolve calcite and plagioclase in the near-well reservoir. Portier et al. [9] established a thermal–hydraulic–chemical (THC) coupling model based on the Soultz EGS project, and the results showed that acidification treatment was beneficial for improving the porosity and permeability of the near reservoir at the site. Na et al. [20] established a one-dimensional reactive solute transport model and simulated the modification effect of CO₂ chemical stimulants on the permeability of geothermal reservoirs under different reaction conditions. Driba et al. [21] conducted a THC coupling simulation based on Phreeqc and OpenGeosys, simulating the impact of injected fluid water chemical composition on the permeability of deep geothermal reservoirs during the process of low-temperature saline reinjection. Regensburg et al. [22] explored the mineral precipitation process during geothermal fluid injection and production using numerical simulation methods.

In this study, the Archaean Baimiao Formation granite in the Matouying uplift area, Tangshan, China, was taken as the target reservoir. TOUGHREACT, a multiphase flow multi-component coupling simulation program, was taken as the simulation tool. A THC reactive solute transport model was established to analyze and predict the reconstruction effect of chemical stimulation with mud acid as the stimulant on the EGS reservoir, as well as the dissolution and precipitation of minerals in the reservoir fractures during the stimulation. The results of this study can provide a design reference and theoretical support for practical ESG reservoir chemical stimulation engineering.

2. Numerical Method

2.1. Simulation Tool

The simulation tool used in this study is TOUGHREACT developed by Lawrence Berkeley State Key Laboratory (Berkeley, CA, USA). The program introduces the reactive solute transport module into the framework of TOUGH2, which is a non-isothermal multi-component flow coupling simulator. The TOUGHREACT can be used for the coupling modeling of underground multiphase fluid and heat flow, solute transport, and chemical reaction in a variety of geological systems and environmental problems, such as geothermal systems, carbon geological storage, pollutant transport, etc. [23]. The thermal physical–chemical process under various conditions such as temperature, pressure, water saturation, and ionic strength was considered in TOUGHREACT. It can be applied to one-dimensional, two-dimensional, and three-dimensional porous and fractured media with physical and chemical heterogeneity, and is applicable to any number of gaseous, liquid, and solid chemical substances. In summary, TOUGHREACT is an ideal simulator for simulating chemical stimulation in EGS reservoir.

2.2. Governing Equations

The fundamental mass and energy balance equations solved by TOUGHREACT can be written in the general form in Equation (1) [24].

$$\frac{d}{dt} \int_{V_n} M dV = \int_{\Gamma_n} F \cdot n d\Gamma + \int_{V_n} q dV \quad (1)$$

where t [s] is the time; n is the grid number; κ is the component number; Γ_n [m²] is the area of connection between grids; V_n [m³] is grid volume; M , F and q are the transport term, source–sink term, and transfer term of mass or energy, respectively.

In the process of fluid–rock interaction, changes in mineral content are controlled by equilibrium (Equations (2) and (3)) and kinetic rates (Equations (4) and (5)) [25].

$$SI_m = \log_{10} \Omega_m = 0 \quad (2)$$

$$\Omega_m = K_m^{-1} \prod_{j=1}^{Nc} c_j^{v_{mj}} \gamma_j^{v_{mj}} \quad m = 1, \dots, Np \quad (3)$$

$$r = A_m k_m \left[1 - \left(\frac{Q}{K} \right)^\mu \right]^n \quad (4)$$

$$k = k_{25}^{nu} \exp \left[\frac{-E_a^{nu}}{R} \left(\frac{1}{T} - \frac{1}{298.15} \right) \right] + k_{25}^H \exp \left[\frac{-E_a^H}{R} \left(\frac{1}{T} - \frac{1}{298.15} \right) \right] \alpha_H^{n_H} + k_{25}^{OH} \exp \left[\frac{-E_a^{OH}}{R} \left(\frac{1}{T} - \frac{1}{298.15} \right) \right] \alpha_{OH}^{n_{OH}} \quad (5)$$

where m is the mineral flag; SI is the saturation index; Ω is saturation; K is the corresponding equilibrium constant; γ is activity coefficient; r [mol/s] is the reaction rate; A [g/cm²] is the reactive specific surface area; k [mol/(L·s)] is the kinetic rate; Q is the reaction quotient; μ and n are the experimental parameters; k_{25} [mol/(L·s)] the reaction rate constant at 25 °C; E_a [KJ/mol] is the activation energy; R [J/mol/K] is the ideal gas constant; T [K] is the temperature; α [mol/L] is the activity.

Porosity changes are directly related to the changes in volume content of minerals. In the TOUGHREACT code, the porosity is given by Equation (7) [26].

$$\varphi = 1 - \sum_{m=1}^{nm} f r_m - f r_u \quad (6)$$

where φ is the porosity; nm is the number of mineral types; fr_m is the volume fraction of mineral m ; fr_u volume fraction of non-reactive minerals.

As fr_m changes, porosity will be recalculated at each time step. TOUGHREACT provides various control equations to describe the mathematical relationship between permeability and porosity changes. Some of them need to call parameters related to changes in crack aperture and pore throat diameter, while the rest are only related to the increase and decrease in porosity. The cubic law (Equation (7)) was taken to calculate the permeability changes caused by an increase or decrease in porosity in this simulation [26].

$$k = k_i \left(\frac{\varphi}{\varphi_i} \right)^3 \quad (7)$$

where k [m^2] is the permeability; k_i [m^2] and φ_i , respectively, refer to initial permeability and porosity.

3. Model Setup

3.1. Geological and Geothermal Setting

The Matouying Uplift area is located in the eastern part of Hebei Province, China, which is a positive secondary structural unit on the northern edge of the Huanghua Platform Depression in the North China Fault Depression, surrounded by the Leting Depression, Nanbao Depression, and Shijiutuo Depression. It is adjacent to the Bozhong Depression to the southeast and the Yanshan Fold Belt to the north, as shown in Figure 1. The main sources of terrestrial heat flow in the study area are mantle-derived heat and heat generated by radioactive decay in rocks within the crust. The development of deep and major faults in the area, such as the Cangdong Fault Zone and the Tanlu Fault Zone, provides a good channel for the upwelling of deep thermal materials [27].

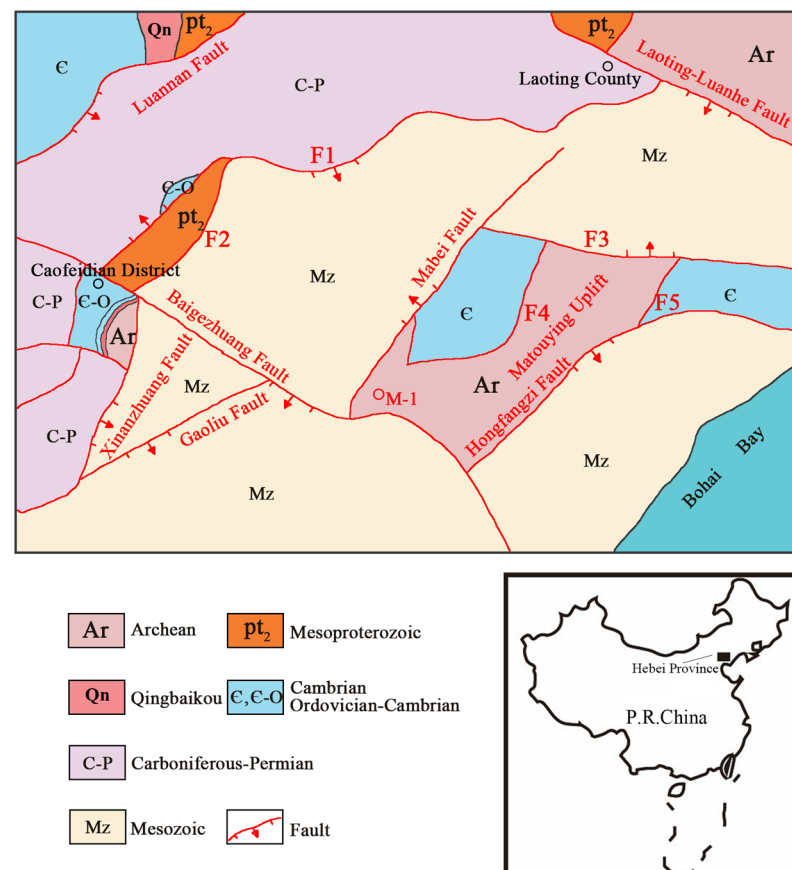


Figure 1. Tectonic location of the study area.

The strata in the study area, from old to new, are sequentially composed of the Cenozoic Quaternary, Neogene and Paleogene, Mesozoic, Paleozoic Ordovician and Cambrian, and Archean. The lithology of the Cenozoic strata is mainly composed of sandstone, fine sandstone, clay rock, siltstone, etc., with good sealing and poor thermal conductivity, forming a good thermal reservoir cover layer, blocking heat flow from deep underground, and keeping the underlying rock mass in a high geothermal environment. The survey results show that the heat flow value in the Matouying uplift area is greater than 75 mW/m^2 , which is higher than the global average heat flow value. The ground temperature gradient is mostly between $3.0\text{--}5.0 \text{ }^\circ\text{C/hm}$, and can reach up to $7.0 \text{ }^\circ\text{C/hm}$ in the central high altitude [28,29].

The granite of the Baimiao Formation in the Archean Dantazi Group in the study area is mainly composed of granulite and shallow-grained rocks [30], with a top boundary buried depth of $1200\text{--}1900 \text{ m}$, a bottom boundary buried depth greater than 4000 m , a thickness of $1500\text{--}2500 \text{ m}$, and a temperature of over $150 \text{ }^\circ\text{C}$. It has high potential for geothermal resource development [31].

3.2. Model Geometry and Spatial Discretization

The conceptual model of this study is shown in Figure 2. The top of the model was located 3900 m below the surface, with a horizontal direction of $102.5 \text{ m} \times 300 \text{ m}$ and a vertical thickness of 102.5 m . The distance between the injection well and production well was set as 200 m , and the fracture extension direction was consistent with the y direction. With reference to relevant research results [20,21], the fracture was generalized to grids with a section size of $2.5 \text{ m} \times 2.5 \text{ m}$. The injection and production wells were located at the leftmost and rightmost ends of the fracture channel, respectively, 50 m away from the boundaries on sides in the x , y , and z directions. Virtual well grids were set to connect them to the fracture grids. For actual chemical stimulation engineering, most of the reaction residues are recovered and treated through production well, with a small portion leaking to distant formations. The production well was set to a constant pressure grid to approximate this process.

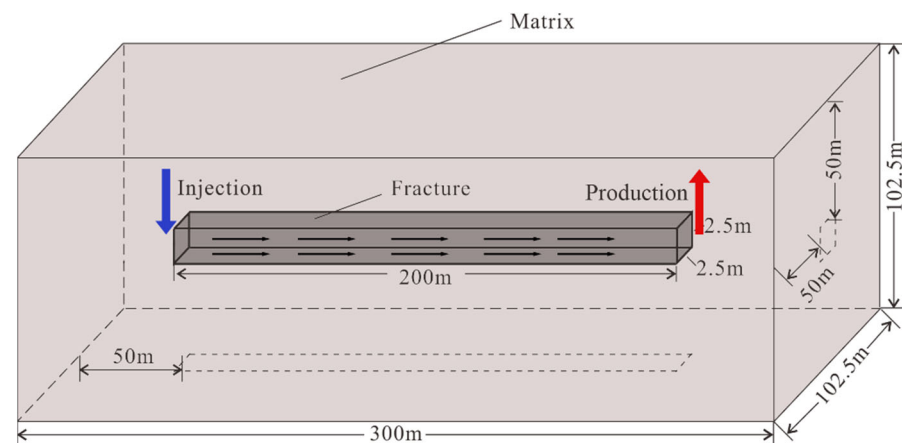


Figure 2. Schematic diagram of conceptual model.

The model was divided into regular three-dimensional Cartesian grids to achieve spatial discretization. The fracture and matrix grids were dissected simultaneously (in subsequent work, these two types of grids were distinguished by modifying lithology parameters), and based on this, the well grids are embedded. Considering that the impact of stimulant injection on the reservoir weakens with the increase in distance from the injection point when conducting mesh generation, the part near the injection point was densified. As the distance from the injection point increases, the generation scale gradually increases from 0.2 m to 15 m .

3.3. Initial and Boundary Conditions

As shown in Figure 2, the vertical thickness of the model is 102.5 m, and the changes in temperature and pressure within this distance are not significant at a depth of about 4000 m. Moreover, chemical stimulants mainly react with minerals inside the fracture channel and adjacent bedrock during the flow process. Therefore, the initial temperature and pressure conditions of the model were uniformly set in this study. Referring to relevant regional surveys and research results [29,31,32], the initial temperature of the model was set to 160 °C, and the initial pressure was set to 40 MPa.

To simulate the injection of a stimulant in different schemes, the fracture grid at the injection site was set as a time-varying Dirichlet boundary. Related studies have shown that the effect of pressure on mineral dissolution and secondary precipitation can be ignored, so this study did not consider the impact of pressure changes during injection on chemical stimulation effects [33–35], and the production side was set as a constant pressure boundary. Due to the short duration of chemical stimulation, the changing regions of temperature and pressure fields do not extend to the boundary. In this simulation, the outer grids of the model were set as infinite volume boundaries, which means that the temperature and pressure at the boundary are constant, to avoid the impact of the model boundary on the simulation results.

3.4. Parameters Setting

3.4.1. Lithologic Parameters

The lithological parameters used in the model are shown in Table 1.

Table 1. Lithologic parameter.

Parameter	Fracture	Matrix
Density (kg/m ³)	2700	2700
Porosity	0.50	0.01
Permeability (m ²)	4.03×10^{-12}	1.43×10^{-15}
Thermal conductivity (W/kg·m)	2.40	2.40
Specific heat capacity (J/K·kg)	653.20	653.20

Among them, the porosity and permeability of fractures and matrix are set according to the models of Na and Xu [12,19], as the other parameters are set according to relevant heat transfer simulation work [36,37]. Initially, the reservoir was set to be homogeneous and isotropic. During the injection process, the porosity and permeability of fractures and surrounding grids change with the dissolution and precipitation of minerals.

3.4.2. Kinetic Parameters for Chemical Reactions

A series of static corrosion experiments and dynamic simulation experiments have been carried out in our previous study [38], to explore the effects of different chemical stimulant formulations (including 10% HCl + 1.5% HF) on deep granite in the Matouying area, and the reaction mechanism between the stimulants and the minerals during the chemical stimulation process was analyzed based on the hydrochemical and microscopic analysis results of samples before and after the reaction. Based on this, the chemical part of the model was set up, and more detailed content can be found in published articles.

According to the XRD mineral composition analysis of the rock sample, the main mineral components of the target reservoir are K-feldspar (30%), plagioclase (33%), quartz (20%), chlorite (15%), and a small amount of biotite (2%). Among them, the content of biotite is only 2%, and according to the results of acid–rock reaction experiments under high temperature and pressure conditions, mud acid with a low concentration had almost no dissolution effect on biotite. Therefore, this study only considered four initial minerals including K-feldspar, plagioclase, chlorite, and quartz (adding 2% non-reactive components in the model to ensure that the content ratio of other initial minerals is the same as the

measured value). According to the results of the dynamic simulation experiment, it can be seen that during the continuous injection of a low concentration of mud acid into the fractures of the granite core, a large amount of amorphous silica was generated in the fracture channels. Therefore, amorphous silica was set as a secondary precipitation mineral in the model, with an initial content of 0.

Based on relevant experimental and numerical studies, [12,18,39], the reaction kinetics parameters of each mineral for different reaction mechanisms are shown in Table 2.

Table 2. Reaction kinetics parameters of minerals.

Mineral	A	Reaction Kinetics Parameters					
		Neutral Mechanism		Acid Mechanism		HF Mechanism	
		K_{25}	E	K_{25}	E	K_{25}	E
Quartz	9.80	1.02×10^{-14}	87.70			2.30×10^{-8}	9.56
K-feldspar	9.80	3.89×10^{-13}	38.00	8.71×10^{-11}	51.70	1.70×10^{-15}	38.90
Albite	4.90	2.75×10^{-13}	69.80	6.92×10^{-11}	65.00	1.90×10^{-5}	32.70
Chlorite	151.00	3.02×10^{-13}	88.00	7.76×10^{-12}	88.00	1.30×10^{-15}	27.89
Amorphous silica	9.80	3.00×10^{-8}	49.80				

4. Simulation Strategy

To explore the effect of acidic chemical stimulants on granite-hosted EGS reservoirs and the influence of different factors on this process, this study simulated the chemical stimulation process under different injection flow rates, injection temperatures, and HF concentrations in this simulation. In the basic scheme, the injection flow rate is 30 kg/s, the injection temperature is 70 °C, and the formula of the stimulant is 10% HCl + 1.5% HF. To further explore the reconstruction effect of chemical stimulation under different injection times and the evolution of mineral content over time during the injection process, global monitoring was conducted on the porosity, permeability, and volume fraction of each mineral in the model at 1 day, 3 days, and 5 days of injection. The specific simulation scheme is shown in Table 3.

Table 3. Simulation strategy.

Scheme Number	Injection Flow Rate (kg/s)	Injection Temperature (°C)	Stimulant Formula
1 (Basic scheme)	30	70	10%HCl + 1.5%HF
2-A	10	70	10%HCl + 1.5%HF
2-B	20	70	10%HCl + 1.5%HF
2-C	40	70	10%HCl + 1.5%HF
3-A	30	60	10%HCl + 1.5%HF
3-B	30	80	10%HCl + 1.5%HF
4-A	30	70	10%HCl + 2.0%HF
4-C	30	70	10%HCl + 2.5%HF

5. Results and Discussion

5.1. Reservoir Reconstruction Effect of Chemical Stimulation

5.1.1. Changes in Temperature and pH

The distribution of temperature and pH in the fracture channel during chemical stimulation lasting for 1 day, 3 days, and 5 days, as well as the changes in temperature and pH over time at different distances from the injection point, are shown in Figure 3. As shown in Figure 3, at the same distance from the injection point, the decrease in temperature significantly lagged behind the change in pH, which means that the response

of the chemical field in the fracture channel to the injection of the stimulant took precedence over the temperature field.

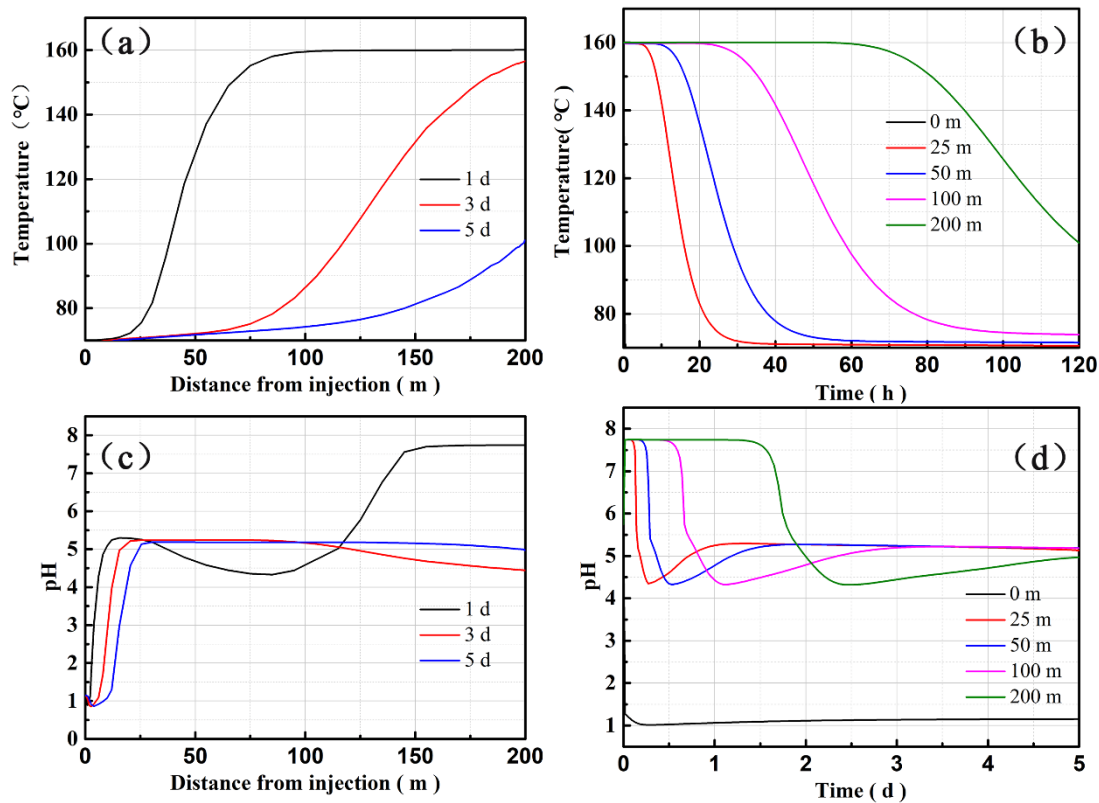


Figure 3. Temperature and pH changes in the fracture channel. (a)-Spatial features of temperature; (b)-Temporal changes in temperature; (c)-Spatial features of pH; (d)-Temporal changes in pH.

Combining Figure 3a,b, it can be seen that when the chemical stimulation lasts for 1 day, the range of temperature reduction had spread to a distance of 105 m from the injection point, and at 60 h (2.5 days), it had spread to the entire fracture channel. The temperature at different distances from the injection point decreased with the continuous occurrence of chemical stimulation and approached equilibrium after a period of time. As the distance from the injection point increased, the duration of this process gradually increased, and the temperature at which it reached stability gradually increased. At 5 d, the temperature at 100 m from the injection point remained stable at around 74 °C, while at 200 m it was still in the process of decreasing. In this simulation, in order to gain a more intuitive understanding of the modification effect of chemical stimulation on reservoir porosity and permeability, we assumed that the continuously injected fluid only migrates through a single fracture channel (surrounded by bedrock with lower porosity and permeability), which resulted in a very fast temperature breakthrough.

From Figure 3c,d, it can be seen that the pH in various parts of the fracture exhibited similar trends. After a period of chemical stimulation, there was a rapid decrease, and after reaching the lowest value, it started to slowly rise, ultimately reaching a near equilibrium state. As the distance from the injection point increases, the time of this process is gradually delayed, and the trend of change gradually eases. This trend of change is caused by the interaction mechanism between the concentration of stimuli and the severity of their interactions with minerals. In the early stage of chemical stimulation, as a large amount of H^+ was injected into the reservoir with a low pH stimulant, the pH value near the well rapidly decreased. However, as the concentration of effective components accumulated, the reaction between the stimulant and the minerals rapidly progressed, and a large amount of H^+ was consumed in the form of HF, causing a slow increase in pH [7]. As the chemical stimulation continued, the reaction between the stimulant and minerals (as the

concentration of H^+) gradually reached a dynamic equilibrium state. Along with the flow process of the stimulant, the response time to this process in various parts of the fracture increased with the distance from the injection point.

5.1.2. Changes in Porosity and Permeability of Fracture

The continuous injection of the chemical stimulant dissolved the minerals in the fracture channel, increasing the porosity of the near wellbore reservoir, and thereby improving permeability. Figure 4 shows the changes in porosity and permeability in the fracture channel near the injection point when chemical stimulation lasted for 1 day, 3 days, and 5 days. As the duration of chemical stimulation continued to extend, the porosity and permeability of the near wellbore fracture channel gradually increased, and the range of significant increases gradually expanded, reflecting that as the minerals in the near wellbore fracture channel continued to be consumed, more stimulant can act on distant formations, achieving longer penetration distances.

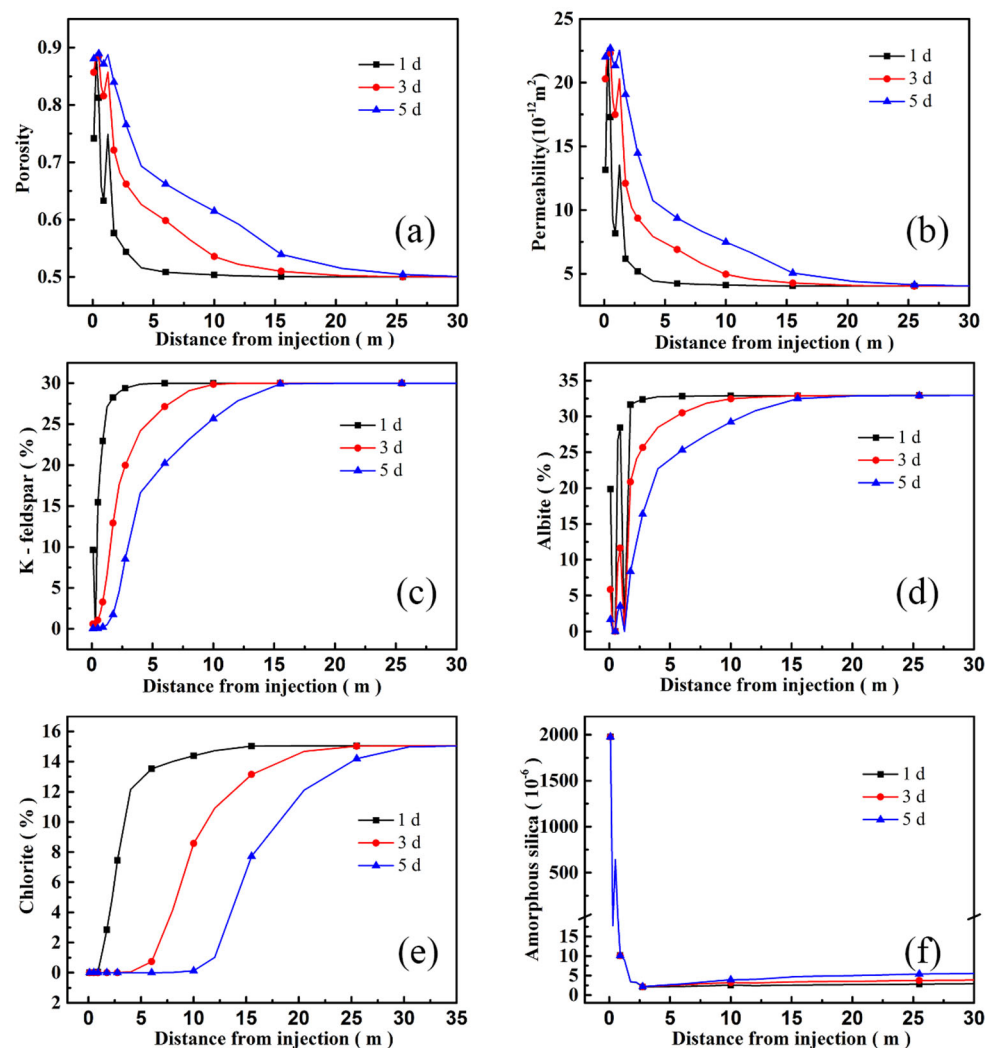


Figure 4. Spatial features at different times. (a)-Porosity distribution at different times; (b)-Permeability distribution at different times; (c)-K-feldspar; (d)-Albite; (e)-Chlorite; (f)-Amorphous silica.

As shown in Figure 4a,b, when the chemical stimulation lasted for 1 day, the effective penetration distance of the stimulant can reach 5 m, and the porosity at 5 m from the injection point can reach 0.52, which is 3.20% higher than the initial value of 0.5, and the permeability can reach $4.43 \times 10^{-12} m^2$, which is 1.10 times the initial value of $4.03 \times 10^{-12} m^2$. At 3 d, the effective penetration distance can reach 17 m, and the porosity at a distance of

5 m from the injection point can reach 0.63, which is 25.29% higher than the initial value, and the permeability can reach $7.93 \times 10^{-12} \text{ m}^2$, which is 1.97 times the initial value; At 5 d, the effective penetration distance can reach 25 m, and the porosity at a distance of 5 m from the injection point can reach 0.69, which is 38.67% higher than the initial value, and the permeability can reach $1.07 \times 10^{-11} \text{ m}^2$, which is 2.67 times the initial value. The improvement effect of the stimulant on the permeability of fracture gradually weakened with the increase in the distance from the injection point and only fluctuated within 1 m near the injection. Within 0.6 m of the injection point, the average porosity of the fracture reached 0.81 at 1 d and did not show significant growth at 3 d and 5 d, reflecting the intense and rapid reaction between minerals and stimulant near the injection point during the initial stage of chemical stimulation, which not only rapidly improved the permeability of the reservoir around the injection point, but also led to the premature depletion of the stimulant and a reduction in penetration.

5.1.3. Changes in Mineral Content

During the process of chemical stimulation, the changes in porosity and permeability of fracture channels are caused by the dissolution and precipitation of reactive minerals. Therefore, it is necessary to monitor and analyze the dissolution and precipitation of various minerals in the fracture channels. In this simulation, four initial minerals (quartz, K-feldspar, albite, and chlorite) and secondary precipitation (amorphous silica) were set. The volume fraction distribution of each mineral at different time nodes is shown in Figure 4. The simulation results show that the volume fraction change in quartz during the entire chemical stimulation process was very weak, which is consistent with the results obtained from relevant experimental studies [17]. Due to the negligible change in quartz content compared to other initial minerals, it is not shown in the figure.

As shown in Figure 4, the content changes in the three main initial minerals are generally similar, and the volume fractions at each location gradually decreased with continuous chemical stimulation. Among them, the volume fraction of chlorite changed the most significantly (Figure 4e), and by 5 days, the reduction range had expanded to 30 m from the injection point, and the chlorite within 10 m near the well had been almost completely dissolved. This is because chlorite, as an acid-sensitive clay mineral [40,41], has a large specific surface area and requires lower activation energy when reacting with the main ingredient HF in the stimulant, making the reaction with the stimulant easier and faster. Based on the analysis in Figure 4, it can be seen that the improvement in permeability of distance formation during the same stimulation time was mainly due to the reaction between chlorite and residual stimulant.

At the same time and at the same distance, the change amplitude in the volume fraction of K-feldspar and albite was obviously lower than that of chlorite (Figure 4c,d). At the same time, the range of volume fraction of the two was very close (albite was slightly farther than K-feldspar), and the reduced area expanded to about 5 m at 1 d and about 15 m at 5 d. Among them, the volume fraction of K-feldspar changed steadily with the distance from the injection point, but the volume fraction of albite fluctuated significantly within 1.5 m near the injection point, which was in negative correlation with the change in porosity and permeability near the well in Figure 4a,b. It can be seen from Figure 4 that the obvious fluctuation of the permeability of the fracture channel near the well was caused by the drastic change in albite content.

In order to further explore the reason for the sharp fluctuation of albite content near the well, the dissolution and precipitation characteristics of albite were set to “dissolution only” [26], and other parameters were consistent with the original scheme. The simulation results are shown in Figure 5. It can be seen from Figure 5 that when there is no secondary albite precipitation in the system, the albite content in the fracture channel monotonously increases with the increase in the distance from the injection point at different time points, so it is believed that the drastic change in albite content and fracture permeability near the well in the original scheme were caused by the secondary albite precipitation.

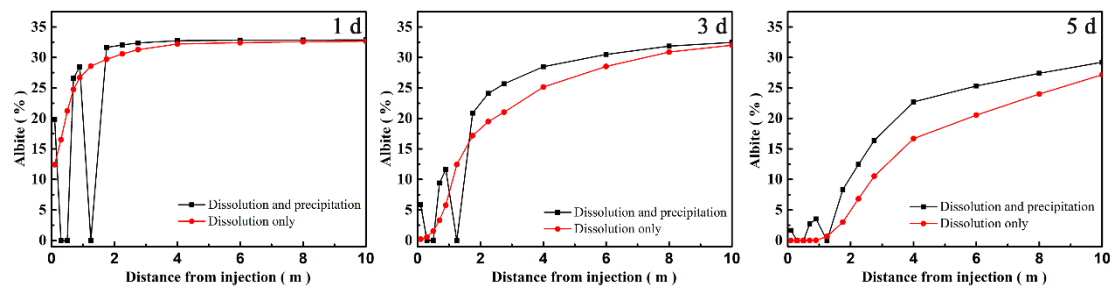


Figure 5. Change in albite content under different constraints.

As shown in Figure 4e, the precipitation of amorphous silica was mainly concentrated within a range of 1 m from the injection point, with a maximum volume fraction of 1.98×10^{-3} , rapidly decreasing to 2×10^{-6} m within a range of 1–5 m, there was a slight increase with the increase in distance from the injection point outside this range, but the precipitation amount near the well can be ignored compared to the precipitation amount near the well. Compared with 1 day, there was no significant change in the amount of amorphous silica precipitation in the fracture channel near the wellbore after stimulation for 3 and 5 days. Therefore, it is believed that the precipitation of amorphous silica mainly occurred within a range of about 1 m near the injection point during the initial stage of chemical stimulation.

5.2. Sensitivity Analysis

5.2.1. Influences of Flow Rate

When the injection temperature was 70°C and the chemical stimulation reached 5 days under different injection flow rates, the changes in porosity and permeability in the fracture channel, and the variables of the volume fractions of each mineral are shown in Figure 6. From Figure 6a,b, it can be seen that with the increase in injection flow rate, the effective penetration distance of chemical stimulation, as well as the porosity and permeability at the same distance from the injection point, had significantly improved. When the injection flow rate increased from 10 kg/s to 40 kg/s , the effective penetration distance increased from 8 m to 30 m after 5 d. The porosity at a distance of 5 m from the injection point has increased from 0.55 to 0.70, an increase of 27.87%, and the permeability has increased from $5.41 \times 10^{-12}\text{ m}^2$ to $1.13 \times 10^{-11}\text{ m}^2$. This is because as the injection flow rate increased, the concentration of the stimulant in the fracture channel near the well became higher, further promoting the forward progress of the dissolution reaction, and facilitating the effective components in the irritant to migrate to the distance at a faster rate. As shown in Figure 6a,b, as the injection flow rate gradually increased, the increase in porosity and permeability near the injection point gradually weakened, while the increase in porosity and permeability further away from the injection point gradually increased. Based on the analysis of the volume fraction changes in minerals, it can be concluded that this is because as chemical stimulation continued, reactive minerals near the injection point were gradually consumed, and more H^+ and HF could be transported to a greater distance.

As shown in Figure 6, within the effective penetration distance, the volume fractions of the three main reactive minerals at the same distance from the injection point decreased with the increase in injection flow rate. Only when the injection flow is increased from 30 kg/s to 40 kg/s , the content change in albite within 2 m near the well did not conform to this trend (Figure 6d). From Figure 6f, it can be seen that the precipitation amount of amorphous silica varies under different injection flow conditions, and the more obvious difference was mainly reflected in the range of 1.5 m near the well. Within the range of 0.4 m from the injection point, the amount of amorphous silica precipitation decreased with the increase in injection flow rate. However, within the range of 0.4–1.5 m from the injection point, when the injection flow rate increased from 10 kg/s to 20 kg/s , the amount of amorphous silica precipitation increased significantly. When the injection flow rate continued to increase to 30 kg/s and 40 kg/s , it decreased again. This was due to the increase in injection flow

rate leading to the intensification of the migration of water chemical components in the fracture channel, which had a certain inhibitory effect on the precipitation of amorphous silica, causing the main location of precipitation to move forward.

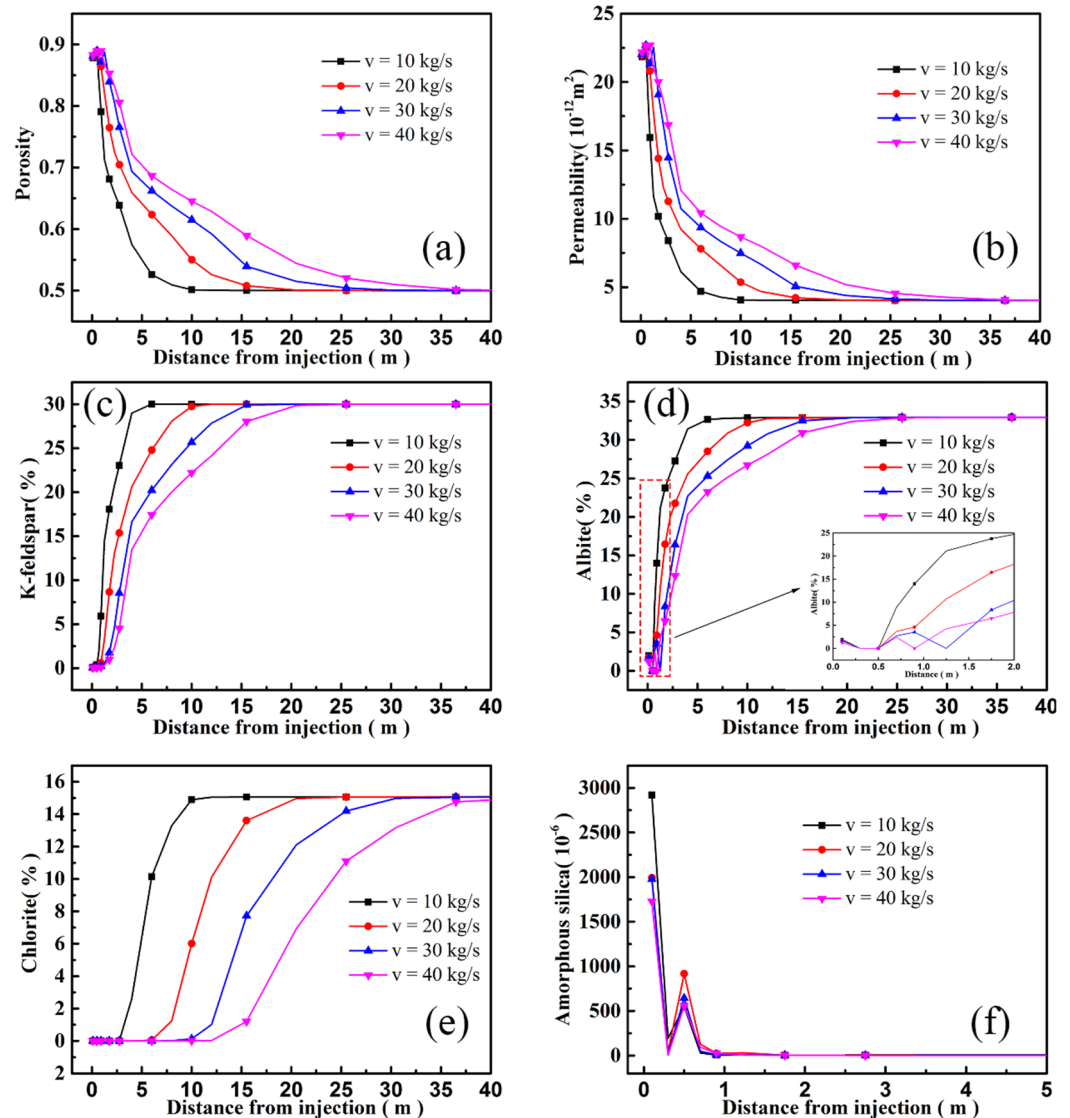


Figure 6. Simulation results at different flow rates. (a)-Porosity distribution at 5 d; (b)-Permeability distribution at 5 d; (c)-K-feldspar; (d)-Albite; (e)-Chlorite; (f)-Amorphous silica.

In summary, increasing the injection flow rate can effectively improve the effectiveness of chemical stimulation for near-wellbore reservoir reconstruction. However, in practical applications, excessive injection flow rate can lead to a rapid increase in injection pressure and an increase in the demand for stimulant dosage, leading to an increase in construction difficulty and cost. Therefore, reasonable adjustments should be made to the injection flow rate of chemical stimulation based on the actual site conditions.

5.2.2. Influences of Injection Temperature

The injection temperature of chemical stimulants may change due to factors such as site conditions and temperature. This study simulates the chemical stimulation process under different injection temperature conditions with an injection flow rate of 30 kg/s. The simulation results for a stimulation time of 5 days are shown in Figure 7. As shown in Figure 7a,b, during the same stimulation time, when the injection temperature was high, the porosity and permeability near the wellbore (within about 13 m) were significantly

improved. This is because the injection fluid with higher temperature had a higher specific enthalpy, which promotes the dissolution reaction of minerals near the wellbore (Figure 7). However, outside the range of 13 m from the injection point, a lower injection temperature achieved better transformation results. This is because high-temperature injection not only promoted the dissolution of near-wellbore minerals but also intensified the consumption of effective components of the stimulants, weakening the corrosion ability of the stimulant to a farther reservoir. As shown in Figure 7c,d, the near-well albite and K-feldspar content decreased with the increase in injection temperature after 5 d, but chlorite was different (Figure 7e). Beyond 7.5 m near the well, its residual content increased with the increase in injection. It can be seen that the increase in injection temperature mainly aggravated the dissolution of feldspar, while the decrease in penetrability was mainly due to the premature consumption of stimulant, which led to the reduction of its dissolution range of chlorite.

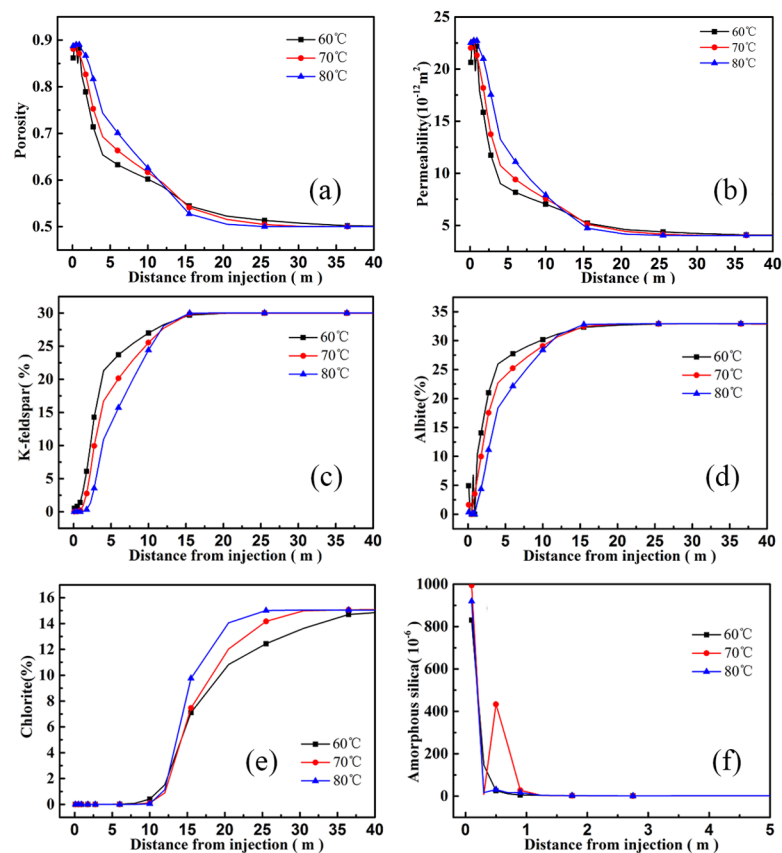


Figure 7. Simulation results at different injection temperatures. (a)-Porosity distribution at 5 d; (b)-Permeability distribution at 5 d; (c)-K-feldspar; (d)-Albite; (e)-Chlorite; (f)-Amorphous silica.

5.2.3. Influences of HF Concentration in Stimulant

Under the condition of injection flow rate of 30 kg/s and injection temperature of 70 °C, the changes in porosity and permeability in the fracture channel after using different HF concentrations of stimulant for 5 days, and the variables of mineral volume fractions are shown in Figure 8. From Figure 8a,b, it can be seen that within the same injection time, the improvement effect of chemical stimulation on the permeability of near wellbore fracture increased with the increase in HF concentration in the stimulant, but the improvement amplitude rapidly weakened beyond a distance of 20 m from the injection point, and the effective penetration distance of the stimulant did not show a significant improvement. As shown in Figure 8c,d, with the increase in HF concentration in the stimulant, the content of feldspar and chlorite in the fracture channel gradually decreased after stimulation, but the effective dissolution distance of the stimulant for the same mineral was almost the same. This is due to the increase in HF concentration, which intensified the reaction between the

stimulant and the nearby reservoir minerals, and the consumption rate of the stimulant accelerated accordingly.

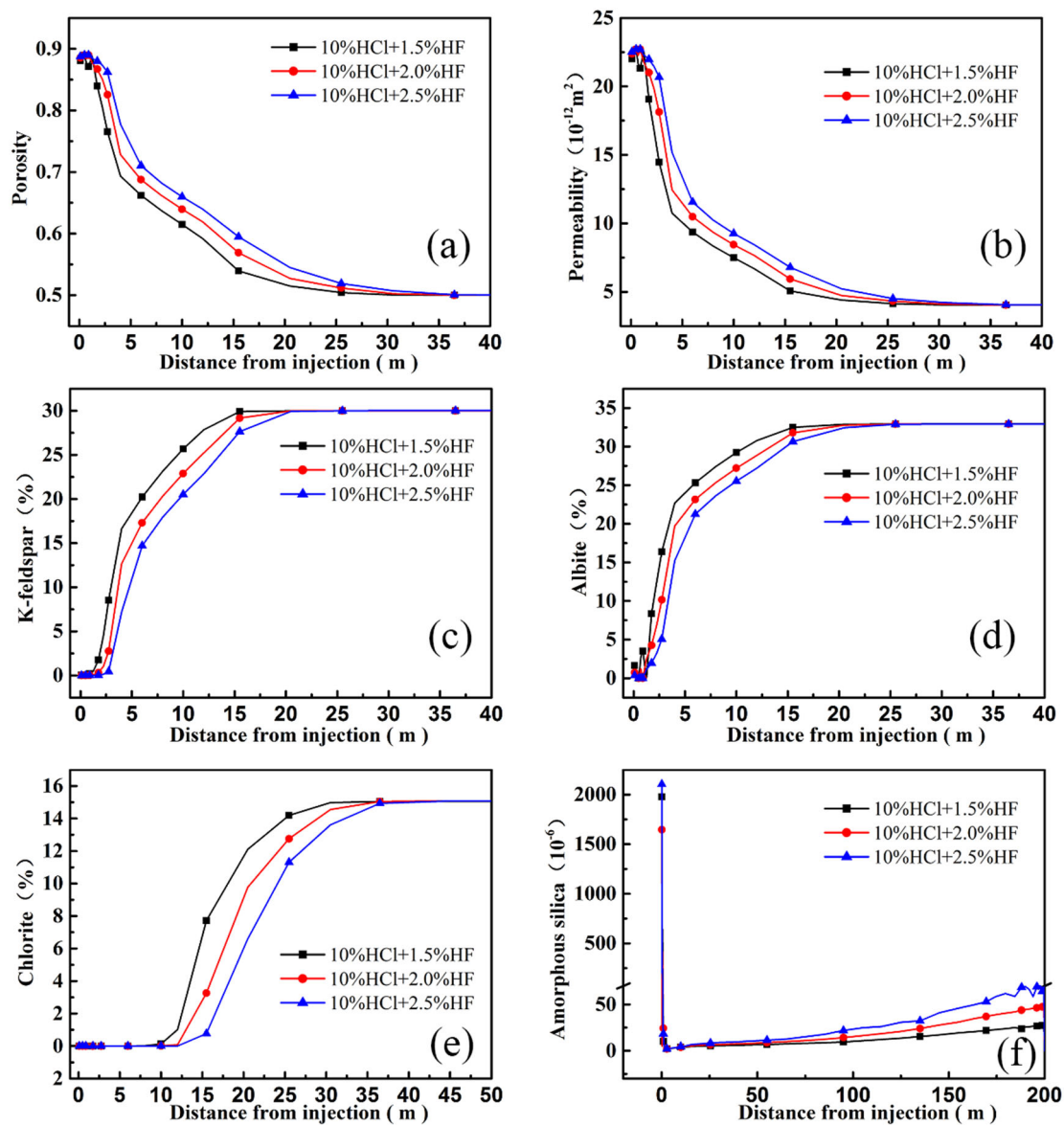


Figure 8. Simulation results at different HF concentrations. (a)-Porosity distribution at 5 d; (b)-Permeability distribution at 5 d; (c)-K-feldspar; (d)-Albite; (e)-Chlorite; (f)-Amorphous silica.

As shown in Figure 8f, the content of amorphous silica in the fracture increased with the increase in HF concentration in the stimulant after stimulation. It can be seen that although higher HF concentration can increase the improvement effect of chemical stimulation on the permeability of the near-well reservoir to a certain extent, it did not have a significant improvement effect on the penetration performance of the stimulant and was more likely to cause secondary precipitation problems. In addition, the difficulty of storing and transporting high-concentration mud acid also needs to be carefully considered.

6. Conclusions

The Archaean Baimiao Formation granite in Matouying uplift area, Tangshan, China, was taken as the target reservoir in this study, and the multiphase flow multi-component coupling simulation program TOUGHREACT was taken as the simulation tool to analyze and predict the reconstruction effect of chemical stimulation with mud acid as the stimulant on EGS reservoir, as well as the dissolution and precipitation of minerals in the reservoir

fractures during the stimulation, to provide design reference and theoretical support for practical ESG reservoir chemical stimulation engineering.

The simulation results show that the chemical stimulation using mud acid as the stimulant can effectively improve the permeability of the near-well reservoir, and the effective penetration distance of 10%HCl + 1.5%HF can reach over 20 m after stimulation for 5 days. The increase in porosity and permeability of the near-well reservoir was mainly attributed to the dissolution of feldspar and chlorite, with the content of chlorite changing particularly significantly. The improvement in permeability of distant formation within the same stimulation time was mainly due to the reaction between chlorite and residual stimulant. The dissolution of quartz was relatively weak and had little effect on the improvement of porosity and permeability. The dissolution and precipitation of albite led to obvious differences in its content at different distances from injection wells, thus causing obvious fluctuations in near-well permeability.

The sensitivity analysis results of operating conditions show that within the same stimulation time, a higher injection flow rate can achieve more significant reconstruction effects through chemical stimulation, while the increase in injection temperature only had an increasing effect on the reservoir porosity and permeability within a certain range near the well (13 m in this simulation) and had a negative impact on the penetration performance of the stimulation agent. A higher concentration of HF can enhance the modification effect of the stimulation agent on the near-well reservoir, but it did not improve its penetration performance and is more likely to cause secondary sedimentation and other problems.

In summary, chemical stimulation has positive significance for ESG reservoir modification, but there are still problems such as rapid stimulant–mineral reaction and limited reconstruction scope. Improving the formula of traditional chemical stimulants, improving their retardancy and penetration, and making them more suitable for high-temperature thermal reservoirs will be an important content of subsequent studies. In addition, this simulation did not consider the impact of mechanical changes caused by pressure and temperature changes during injection on reservoir permeability. How to achieve coupling between mechanical processes and reactive solute transport is also a direction worth exploring and researching.

Author Contributions: Conceptual model and numerical simulation, L.M. and Z.C.; visualization and writing, B.F.; sample collection and data acquisition, X.Q. and Y.Z.; funding acquisition and resources administration, C.Z. All authors have read and agreed to the published version of the manuscript.

Funding: This work was supported by the Engineering Research Center of Geothermal Resources Development Technology and Equipment, Ministry of Education, Jilin University, and the comprehensive survey of natural resources in the middle reaches of the Yitong River (DD20220867).

Data Availability Statement: The original contributions presented in the study are included in the article, and further inquiries can be directed to the corresponding author.

Acknowledgments: The authors would like to extend their sincere gratitude to the relevant institutions for financial and technical support.

Conflicts of Interest: The authors declare no conflict of interest.

References

1. Barcelona, H.; Senger, M.; Yagupsky, D. Resource assessment of the Copahue geothermal field. *Geothermics* **2021**, *90*, 101987. [[CrossRef](#)]
2. Kharseh, M. Optimizing Geothermal Energy Resource. *J. Mech. Eng. Autom.* **2015**, *5*, 667–675.
3. Lv, Y.; Yuan, C.; Zhu, X.; Gan, Q.; Li, H. THMD analysis of fluid injection-induced fault reactivation and slip in EGS. *Geothermics* **2022**, *99*, 102303. [[CrossRef](#)]
4. Portier, S.; Vuataz, F.D.; Nami, P.; Sanjuan, B.; Gerard, A. Chemical stimulation techniques for geothermal wells: Experiments on the three-well EGS system at Soultz-sous-Forets, France. *Geothermics* **2009**, *38*, 349–359. [[CrossRef](#)]
5. Mahmoodpour, S.; Singh, M.; Bär, K.; Sass, I. Impact of Well Placement in the Fractured Geothermal Reservoirs Based on Available Discrete Fractured System. *Geosciences* **2022**, *12*, 19. [[CrossRef](#)]

6. Siratovich, P.A.; Villeneuve, M.C.; Cole, J.W.; Kennedy, B.M.; Begue, F. Saturated heating and quenching of three crustal rocks and implications for thermal stimulation of permeability in geothermal reservoirs. *Int. J. Rock Mech. Min. Sci.* **2015**, *80*, 265–280. [[CrossRef](#)]
7. Na, J.; Xu, T.F.; Jiang, Z.J.; Bao, X.H.; Wu, Y.D.; Feng, B. A study on the interaction of mud acid with rock for chemical stimulation in an enhanced geothermal system. *Environ. Earth Sci.* **2016**, *75*, 1025. [[CrossRef](#)]
8. Feng, B.; Xu, J.N.; Xu, T.F.; Li, S.T.; Song, D.; Chen, M.T. Application and Recent Progresses of Chemical Stimulation on Hot Dry Rock Reservoir Modification. *J. Earth Sci. Environ.* **2019**, *41*, 577–591.
9. Portier, S.; Vuataz, F.D. Developing the ability to model acid-rock interactions and mineral dissolution during the RMA stimulation test performed at the Soultz-sous-Forets EGS site, France. *Comptes Rendus Geosci.* **2010**, *342*, 668–675. [[CrossRef](#)]
10. Mahmoodpour, S.; Singh, M.; Obaje, C.; Tangirala, S.K.; Reinecker, J.; Bär, K.; Sass, I. Hydrothermal Numerical Simulation of Injection Operations at United Downs, Cornwall, UK. *Geosciences* **2022**, *12*, 296. [[CrossRef](#)]
11. Grigsby, C. Interaction of granite with aqueous sodium carbonate. *Trans.-Geotherm. Resour. Counc.* **1977**, *1*, 64–71.
12. Na, J. Study of Chemical Stimulation on the Enhanced Geothermal Systems (EGS) in Yingcheng Formation of Songliao Basin, China. Ph.D. Thesis, Jilin University, Changchun, China, 2016.
13. Liu, M.L.; Zhuang, Y.Q.; Zhou, C.; Zhu, M.C.; Zhang, C.H.; Zhu, Y.Q.; Tan, L.; Luo, J.; Guo, Q.H. Application of chemical stimulation technology in enhanced geothermal system: Theory, practice and expectation. *J. Earth Sci. Environ.* **2016**, *38*, 267–276.
14. Eliasson, T.; Schöeberg, H. U-Pb dating of the post-kinematic Sveconorwegian (Grenvillian) Bohus granite, SW Sweden: Evidence of restitic zircon. *Precambrian Res.* **1991**, *51*, 337–350. [[CrossRef](#)]
15. Fei, Y. Acidizing Sandstone Reservoirs Using HF and Organic Acids. Master's Thesis, Texas A&M University, College Station, TX, USA, 2012.
16. Na, J.; Xu, T.F.; Wu, Y.D.; Feng, B.; Bao, X.H. Effectiveness of using mud acid as stimulation agent for enhanced geothermal systems (EGS) reservoir. *J. Cent. South Univ. Sci. Technol.* **2017**, *48*, 247–254.
17. Luo, J.; Zhu, Y.Q.; Guo, Q.H.; Tan, L.; Zhuang, Y.Q.; Liu, M.L.; Zhang, C.H.; Zhu, M.C.; Xiang, W. Chemical stimulation on the hydraulic properties of artificially fractured granite for enhanced geothermal system. *Energy* **2018**, *142*, 754–764. [[CrossRef](#)]
18. Yue, G.F.; Li, X.Y.; Gan, H.N.; Wang, G.L. A study on the reaction kinetics of regular mud acid and granite. *Acta Geol. Sin.* **2020**, *94*, 2108–2114.
19. Xu, T.; Rose, P.; Fayer, S.; Pruess, K. On modeling of chemical stimulation of an enhanced geothermal system using a high pH solution with chelating agent. *Geofluids* **2009**, *9*, 167–177. [[CrossRef](#)]
20. Na, J.; Feng, B.; Lan, C.Y.; Xu, T.F.; Bao, X.H. Effectiveness of using supercritical CO₂ as stimulation agent for enhanced geothermal systems. *J. Cent. South Univ. Sci. Technol.* **2014**, *45*, 2447–2458.
21. Driba, D. 1D Thermal-Hydraulic-Chemical (THC) Reactive transport modeling for deep geothermal systems: A case study of Groß Schönebeck reservoir, Germany. In Proceedings of the AGU Fall Meeting, San Francisco, CA, USA, 15–19 December 2014.
22. Regenspurg, S.; Feldbusch, E.; Byrne, J.; Deon, F.; Driba, D.L.; Henniges, J.; Kappler, A.; Naumann, R.; Reinsch, T.; Schubert, C. Mineral precipitation during production of geothermal fluid from a Permian Rotliegend reservoir. *Geothermics* **2015**, *54*, 122–135. [[CrossRef](#)]
23. Shi, X.Q.; Zhang, K.N.; Wu, J.C. The history and application of TOUGH2 code. *Geotech. Investig. Surv.* **2009**, *37*, 29–34, 39.
24. Feng, G.; Xu, T.; Zhao, Y.A.; Gherardi, F. Heat mining from super-hot horizons of the Larderello geothermal field, Italy. *Renew. Energy* **2022**, *197*, 371–383. [[CrossRef](#)]
25. Xu, J.N.; Feng, B.; Cui, Z.P.; Liu, X.Y.; Ke, Z.S.; Feng, G.H. Comparative Study of Acid and Alkaline Stimulants with Granite in an Enhanced Geothermal System. *Acta Geol. Sin. Engl. Ed.* **2021**, *95*, 1926–1939. [[CrossRef](#)]
26. Xu, T.; Spycher, N.; Sonnenthal, E.; Zhang, G.; Zheng, L.; Pruess, K. TOUGHREACT Version 2.0: A simulator for subsurface reactive transport under non-isothermal multiphase flow conditions. *Comput. Geosci.* **2011**, *37*, 763–774. [[CrossRef](#)]
27. Zhang, B.J.; Li, Y.Y.; Gao, J.; Wang, G.L.; Li, Y.; Xing, Y.F.; Zhao, T. Genesis and indicative significance of hot dry rock in Matouying, Hebei Province. *Acta Geol. Sin.* **2020**, *94*, 2036–2051.
28. Shangguan, S.T. Occurrence conditions of hot-dry-rock geothermal resources and development prospects in Matouying area. *China Energy Environ. Prot.* **2017**, *39*, 155–165.
29. Qi, X.F.; Shangguan, S.T.; Zhang, G.B.; Pan, M.M.; Su, Y.; Tian, L.L.; Li, X.; Qiao, Y.C.; Zhang, J.Y. Site selection and developmental prospect of a hot dry rock resource project in the Matouying Uplift, Hebei Province. *Earth Sci. Front.* **2020**, *27*, 94–102.
30. Zhao, Y.H.; Feng, B.; Zhang, G.B.; Shangguan, S.T.; Qi, X.F.; Li, X.; Qiao, Y.C.; Xu, J.N. Study of the interaction between the granitic hot-dry rock (HDR) and different injection waters. *Acta Geol. Sin.* **2020**, *94*, 2115–2123.
31. Qi, X.F.; Zhang, G.B.; Shangguan, S.T.; Su, Y.; Tian, L.L.; Li, X.; Qiao, Y.C.; Liu, X. A Brief Analysis of Hot and Dry Rock Geothermal Resources Hosting and Distribution in Hebei Province. *Coal Geol. China* **2018**, *30*, 47–73.
32. Shangguan, S.T.; Sun, D.S.; Zhang, G.B.; Yang, Y.H.; Qi, X.F.; Chen, D.F.; Qiao, Y.C.; Li, A.W.; Chen, Q.C. In-situ stress measurement and fault stability analysis within a depth of 3~4 km in the Tangshan area. *Acta Geol. Sin.* **2021**, *95*, 3915–3925.
33. Xu, Z.M. Hydrochemistry of silicate rock slope. *J. Geol.* **2013**, *87*, 860–871.
34. Shi, Y.F.; Xu, T.F.; Wang, F.G.; Feng, G.H.; Tian, H.L.; Lei, H.W. Water rock gas interaction in carbon dioxide plume geothermal system: A case study of Quantou Formation in Songliao basin. *J. Jilin Univ. Earth Sci. Ed.* **2014**, *44*, 1980–1987.
35. Chen, Y.L.; Tian, T.; Qi, F.M. Application of Compatibility Experiment in Geothermal Re-irrigation Test in Xi'an. *Groundwater* **2011**, *33*, 25–26.

36. Feng, B.; Cui, Z.P.; Zhao, P.; Liu, X.; Hu, Z.X. Numerical simulation of heating potential of U-shaped geothermal well based on T2WELL. *J. Jilin Univ. Earth Sci. Ed.* **2022**, *52*, 560–570.
37. Xu, T.F.; Hu, Z.X.; Feng, B.; Feng, G.H.; Li, F.Y.; Jiang, Z.J. Numerical evaluation of building heating potential from a co-axial closed-loop geothermal system using wellbore–reservoir coupling numerical model. *Energy Explor. Exploit.* **2020**, *38*, 733–754. [[CrossRef](#)]
38. Cui, Z.; Shangguan, S.; Gherardi, F.; Qi, X.; Xu, J.; He, S.; Feng, B. Experimental Study on the Effect and Mechanism of Chemical Stimulation on Deep High-Temperature Granite. *Front. Earth Sci.* **2022**, *10*, 893969. [[CrossRef](#)]
39. Xu, T.; Senger, R.; Finsterle, S. Bentonite Alteration Due to Thermal-Hydro-Chemical Processes During the Early Thermal Period in a Nuclear Waste Repository. *Nucl. Technol.* **2011**, *174*, 438–451. [[CrossRef](#)]
40. Tang, H.M.; Zhang, F.; Li, G.; Wang, C.H.; Xie, X.Y. Distributory Multiple Hydrofracturing of Horizontal Wells in Daqing Oil Field. *Oilfield Chem.* **2007**, *24*, 307–309.
41. Kamal, M.S.; Mahmoud, M.; Hanfi, M.; Elkatatny, S.; Hussein, I. Clay minerals damage quantification in sandstone rocks using core flooding and NMR. *J. Pet. Explor. Prod. Technol.* **2019**, *9*, 593–603. [[CrossRef](#)]

Disclaimer/Publisher’s Note: The statements, opinions and data contained in all publications are solely those of the individual author(s) and contributor(s) and not of MDPI and/or the editor(s). MDPI and/or the editor(s) disclaim responsibility for any injury to people or property resulting from any ideas, methods, instructions or products referred to in the content.